Ultramicroscopy 108 (2008) 1546–1550

Contents lists available at ScienceDirect

Ultramicroscopy

journal homepage: www.elsevier.com/locate/ultramic

Dynamical effects of anisotropic inelastic scattering in electron backscatter diffraction

Aimo Winkelmann *

Max-Planck-Institut für Mikrostrukturphysik, Weinberg 2, D-06120 Halle, Germany

ARTICLE INFO

Article history:
Received 21 January 2008
Received in revised form
28 April 2008
Accepted 6 May 2008

Keywords:
Electron backscatter diffraction

ABSTRACT

We present a model which describes the appearance of excess and deficiency features in electron backscatter diffraction (EBSD) patterns and we show how to include this effect in many-beam dynamical simulations of EBSD. The excess and deficiency features appear naturally if we take into account the anisotropy of the internal source of inelastically scattered electrons which are subsequently scattered elastically to produce the EBSD pattern. The results of simulations applying this model show very good agreement with experimental patterns. The amount of the excess–deficiency asymmetry of the Kikuchi bands depends on their relative orientation with respect to the incident beam direction. In addition, higher order Laue zone rings are also influenced by the same effect.

1. Introduction

Electron backscatter diffraction (EBSD) is a valuable tool for the analysis of crystalline materials on the nanometer scale [1,2]. An EBSD pattern can be thought of as created by point-like sources of backscattered electrons inside the crystal. From these sources, electrons are emitted into all directions. Subsequently, they are scattered elastically and inelastically by the surrounding atoms and the modulation of their probability to reach the detection screen shows up as the EBSD pattern. We have recently demonstrated how to simulate realistic EBSD patterns using the dynamical theory of electron diffraction [3].

While a theoretical description of electron diffraction in terms of spherical waves emanating from point sources is possible and heavily used in low energy electron diffraction and related techniques [4], at high energies it is more efficient to apply the reciprocity principle and use a description in terms of *ingoing* plane waves and to look for the intensity at the positions of the internal sources. It turns out that the corresponding diffraction problem is basically the same as in convergent beam electron diffraction in the transmission electron microscope. This fact allowed us to apply existing Bloch wave approaches [5,6] to calculate the diffracted wave function inside the crystal with the additional extension of the corresponding algorithms to describe the initial inelastic scattering processes constituting the internal sources for the EBSD pattern.

In a first approximation, we assumed that the initial inelastic scattering process can be sufficiently well described by isotropic scattering located at the atomic positions and scaling with the atomic number as Z^2. This assumption amounts basically to an integration of the intensity at the atomic positions broadened by thermal vibrations. It was also assumed that, effectively, the diffraction at a single energy near the energy of the incident beam is dominating the experimental EBSD patterns. While we could demonstrate very good agreement between experimental patterns taken at 20 kV from GaN(0 0 0 1) and patterns simulated under the above simplifying assumptions, it would be clearly be important to analyze the effects of inelastic scattering more closely.

Two types of improvements of our previous simulations suggest themselves: first, the inclusion of the energy spread of the backscattered electrons; second, the inclusion of the angular anisotropy of the inelastic scattering. We assume here that both types of influences can be handled independently in a first approximation. The second effect is qualitatively different from the first with respect to necessary modifications of the model used for the simulation, and this will be the main topic of the present paper. We comment shortly on the effect of the back-scattered electron energy spectrum in the concluding Section 4.

What kind of qualitative changes can be expected if we take into account that the incident electrons are inelastically scattered with different intensity into different directions? The scattering at high kinetic energies is strongly enhanced in the forward direction. Due to the geometry of EBSD experiments with shallow incidence angles, a significant anisotropy of the initial distribution of the produced inelastic electrons exists with respect to the detected directions. First of all, the accumulated incoherent

* Tel.: +49 345 5582639; fax: +49 345 5511223.
E-mail address: winkelm@mpi-halle.mpg.de

0304-3991/$ - see front matter © 2008 Elsevier B.V. All rights reserved.
doi:10.1016/j.ultramic.2008.05.002

multiple inelastic scattering processes result in the anisotropic large angular scale intensity distribution of the observed unprocessed EBSD patterns, which show higher intensity near the forward scattering direction of the incident beam and much lower intensity towards the backscattering directions. The variations introduced in this way are of a much larger angular size than the angular extension of the Kikuchi lines and bands, which means that the relatively slowly varying kinematic background can be removed by flat-fielding techniques.

More importantly, the anisotropy of each individual inelastic scattering event (which produces a coherent electron wave starting from the backscattering atom) also enters into the dynamical diffraction problem and results in selective enhancement or suppression of the intensity of Kikuchi lines as a function of their orientation with respect to the incoming beam direction. The mechanism of these excess and deficiency lines has been explained long ago for the case of transmission electron microscopy (TEM) Kikuchi patterns [7]. Here, the incident beam can be directly observed and its influence is experimentally rather obvious. The incident beam in EBSD, in contrast, is not directly observed. But very similar to the TEM case, it acts to create anisotropic sources of inelastically scattered electrons which produce the Kikuchi patterns.

The excess lines usually appear at scattering angles which are farther away from the incident beam direction than the deficiency lines. If the inelastically scattered electrons with wave vectors near the incident beam direction have a higher intensity than the wave vectors for larger scattering angles, intensity is then asymmetrically removed by diffraction from the position of the deficiency line and transferred to the excess line. This process will be explained in the next section. A mathematical model is then extracted and applied to many-beam dynamical simulations which show excellent agreement with experimental observations.

The main aim of this paper is to provide—for the cost of some reasonable approximations—a clear physical picture of the mechanism behind the excess–deficiency features in EBSD patterns and to point out the directions along which possible improvements can be implemented for future quantitative investigations. In this way, we hope to contribute to an improved understanding of the various aspects of EBSD pattern intensities.

2. Qualitative description

In Fig. 1, we show the basic ingredients that are necessary to qualitatively understand the excess–deficiency effect in EBSD.

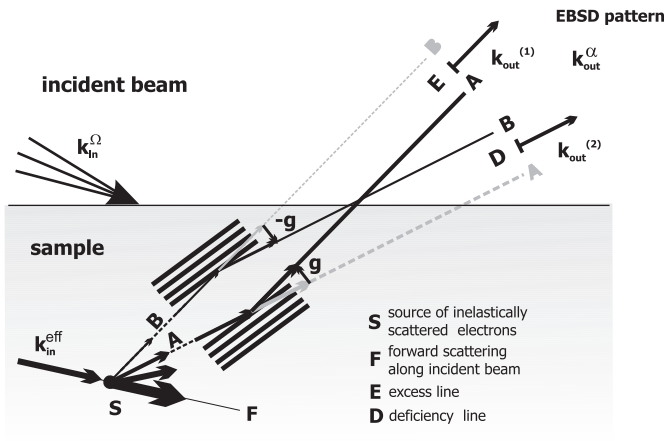

Fig. 1. Mechanism of the formation of excess and deficiency lines in EBSD patterns.

Sources **S** of inelastically backscattered electrons are localized at atomic positions inside the crystal. The creation of inelastic electrons is not isotropic, and different amounts of electrons are backscattered into the directions *A* and *B*. In the theoretical model to be described later, we will for simplicity assume that the relative strength of backscattering (corresponding to the thickness of the arrows in Fig. 1) can be described by a simple Gaussian dependence as a function of the deviation of the scattering direction from forward scattering **F** along an effective incidence direction $\mathbf{k}_{\mathrm{in}}^{\mathrm{eff}}$. What is important for the mechanism of the effect is only that a difference exists between the amounts of electrons that are initially excited into the different directions *A* and *B*. Subsequently, these electrons are dynamically diffracted by the surrounding crystal lattice. In Fig. 1, we show the case that beams along *A* will be scattered by lattice plane **g**, whereas beams along *B* will be scattered by $-\mathbf{g}$, corresponding to a pair of Kikuchi lines. The intensities along $\mathbf{k}_{\mathrm{out}}^{(1)}$ and $\mathbf{k}_{\mathrm{out}}^{(2)}$ in the EBSD pattern can be thought to be formed by electrons that are moving into these directions without scattering, plus electrons that are dynamically scattered from other initial directions into these final directions. Assuming equally strong scattering by **g** and $-\mathbf{g}$, the dynamical diffraction problem is perfectly symmetric. Similarly, the dynamically diffracted intensities in the directions $\mathbf{k}_{\mathrm{out}}^{(1)}$ and $\mathbf{k}_{\mathrm{out}}^{(2)}$ would be equal and would not show an excess–deficiency asymmetry if we had the same number of *A* and *B* electrons. Now we consider that *A* is initially stronger than *B*. We see in Fig. 1 that, because there are more *A* than *B* electrons, a higher number of electrons are necessarily scattered by **g** away from the initial direction of the *A* electrons into the direction $\mathbf{k}_{\mathrm{out}}^{(1)}$ than the number of *B* electrons that is scattered by $-\mathbf{g}$ from $\mathbf{k}_{\mathrm{out}}^{(1)}$ back to the initial *A* direction $\mathbf{k}_{\mathrm{out}}^{(2)}$. By this mechanism more intensity ends up in direction $\mathbf{k}_{\mathrm{out}}^{(1)}$ than in direction $\mathbf{k}_{\mathrm{out}}^{(2)}$, forming the excess *E* and deficiency *D* feature, respectively. This qualitative description will now be cast into a theoretical model.

3. Theoretical modelling

To clarify the notation, we will first give a short summary of the general approach we apply.

We need to describe the relative intensity distribution of backscattered electrons on the phosphor screen used for detection. The corresponding range of outgoing wave vectors is denoted by $\mathbf{k}_{\mathrm{out}}^{\alpha}$ where α labels the direction towards a point on the phosphor screen in a suitably chosen coordinate system. A Bloch wave approach is used to describe the diffraction of electrons travelling along the directions $\mathbf{k}_{\mathrm{out}}^{\alpha}$ [5,6]. The wave function inside the crystal is described as a superposition of Bloch waves with wave vectors $\mathbf{k}^{(j)}$:

$$\Psi(\mathbf{r}) = \sum_j c_j \exp(\mathrm{i}\mathbf{k}^{(j)} \cdot \mathbf{r}) \sum_{\mathbf{g}} C_{\mathbf{g}}^{(j)} \exp(\mathrm{i}\mathbf{g} \cdot \mathbf{r}) \tag{1}$$

For a specific $\mathbf{k}_{\mathrm{out}}^{\alpha}$ outside the crystal, we can determine the electron wave vector **K** inside the crystal which is used to express $\mathbf{k}^{(j)}$ as $\mathbf{k}^{(j)} = \mathbf{K} + \lambda^{(j)}\mathbf{n}$ where **n** is a unit vector normal to the surface. Starting from the Schrödinger equation, one can then set up an eigenvalue problem [5] which gives the eigenvalues $\lambda^{(j)}$ and eigenvectors with elements $C_{\mathbf{g}}^{(j)}$. The boundary conditions at the surface determine the coefficients c_j in Eq. (1). After this, the wave function Eq. (1) is known and can be used to calculate the electron probability density inside the crystal for a plane wave moving in the $\mathbf{k}_{\mathrm{out}}^{\alpha}$ direction. For each pixel on the detection plane, a separate calculation is carried out.

The dynamical diffraction part of the cross-section of the localized scattering processes can be written as [8]

$$I_{\mathrm{DYN}} \propto \sum_{i,j} B^{ij}(t) \sum_{\mathbf{g},\mathbf{h}} C_{\mathbf{g}}^{(i)} C_{\mathbf{h}}^{(j)*} \mu_{\mathbf{g},\mathbf{h}} \tag{2}$$

with a depth integrated interference term $B^{ij}(t)$ of the Bloch waves i and j:

$$B^{ij}(t) = c_i c_j^* \frac{\exp[\mathrm{i}(\lambda^i - \lambda^{j*})t] - 1}{\mathrm{i}(\lambda^i - \lambda^{j*})t} \tag{3}$$

The terms $\mu_{\mathbf{g},\mathbf{h}}$ describe the matrix elements of the inelastic process of interest. The EBSD patterns can be well described by considering thermal diffuse scattering described within an Einstein model [9]. For a wave-vector transfer $\mathbf{q}$ from an incident beam direction $\mathbf{k}_{\mathrm{in}}$ to a direction $\mathbf{k}_{\mathrm{out}}^{\alpha}$ towards the phosphor screen, the $\mu_{\mathbf{g},\mathbf{h}}$ are proportional to [8]

$$\mu_{\mathbf{g},\mathbf{h}}(\mathbf{k}_{\mathrm{in}}, \mathbf{k}_{\mathrm{out}}^{\alpha}) \propto \sum_n \exp[\mathrm{i}(\mathbf{g}-\mathbf{h})\cdot\mathbf{r}_n] f_n(\mathbf{q}+\mathbf{g}) f_n(\mathbf{q}+\mathbf{h}) \times [\exp(-M_{\mathbf{g}-\mathbf{h}}^n) - \exp(-M_{\mathbf{q}+\mathbf{g}}^n - M_{\mathbf{q}+\mathbf{h}}^n)] \tag{4}$$

For backscattering corresponding to very large $\mathbf{q} \gg \mathbf{g}, \mathbf{h}$, in Eq. (4) one can make the approximation that the scattering factor f_n does not vary between wave vector transfers $\mathbf{q}$ and $\mathbf{q}+\mathbf{g}$: $f_n(\mathbf{q}+\mathbf{g}) \approx f_n(\mathbf{q})$. With $f_n \propto Z_n$ this leads to a factor Z_n^2 in the cross section. Furthermore, only the Debye–Waller terms $\exp(-M_{\mathbf{g}-\mathbf{h}}^n)$ are significant.

For an incident focussed probe beam of sufficient angular divergence one has to integrate over all incident beam wave vectors $\mathbf{k}_{\mathrm{in}}^{\Omega}$ that contribute to intensity scattered to the direction $\mathbf{k}_{\mathrm{out}}^{\alpha}$ via corresponding scattering vectors $\mathbf{q}^{\mathbf{\Omega}}$. Here, Ω describes an angular range of incident wave vectors and the corresponding integration results in the geometrical factor A (see Ref. [8], Eq. (10)) in the cross section formula which we have used for our previous simulations [3]:

$$I_{\mathrm{DYN}} \propto A \sum_{n,ij} Z_n^2 B^{ij}(t) \sum_{\mathbf{g},\mathbf{h}} C_{\mathbf{g}}^{(i)} C_{\mathbf{h}}^{(j)*} \exp(-M_{\mathbf{g}-\mathbf{h}}^n) \exp[\mathrm{i}(\mathbf{g}-\mathbf{h})\cdot\mathbf{r}_n] \tag{5}$$

with atoms at $\mathbf{r}_n$.

Using the method described above, we have obtained unprecedented agreement of simulated patterns with experimental EBSD patterns [3]. However, the experimentally observed excess–deficiency features were not reproduced using this approximation. The reason obviously is connected to the fact that the properties of the incident beam do not appear anymore in Eq. (5) except for the constant geometrical factor A. From the discussion of the simplified physical picture in the previous section, we saw that the strongly anisotropic forward inelastic scattering with some scattering angles well below 90° from the incident direction is the cause of the excess–deficiency effect. Obviously, our assumption that the scattering factor f_n does not vary between wave-vector transfers $\mathbf{q}$ and $\mathbf{q}+\mathbf{g}$ has to be dropped, and in Eq. (4) it needs to be considered that $f_n(\mathbf{q}+\mathbf{g}) \neq f_n(\mathbf{q}+\mathbf{h})$.

We now look for a transparent way to incorporate the anisotropy of the inelastic scattering into an equation of the type of Eq. (5). Because we do not want to describe the microscopic details of the multiple inelastic and elastic scattering of the incident beam, we assume in a first approximation that we are still looking only at quasi-elastically scattered electrons but that, in the many-beam problem, the beams $\mathbf{g}$ are excited with different strengths according to an appropriately chosen function χ that depends on $\mathbf{g}$ and the incident and detected beam directions:

$$f_n(\mathbf{q}+\mathbf{g}) \propto Z_n \cdot \chi_{\mathbf{g}}(\mathbf{k}_{\mathrm{in}}, \mathbf{k}_{\mathrm{out}}^{\alpha}) \tag{6}$$

For simplicity, we assume that the relative strength of excitation shows a Gaussian distribution as a function of wave-vector transfer $\mathbf{q}$ from some effective incident beam direction $\mathbf{k}_{\mathrm{in}}^{\mathrm{eff}}$:

$$\chi_{\mathbf{g}} = 1 + a \cdot \exp\left(\frac{-(\mathbf{k}_{\mathrm{out}}^{\alpha} - \mathbf{k}_{\mathrm{in}}^{\mathrm{eff}} + \mathbf{g})^2}{b^2}\right) \tag{7}$$

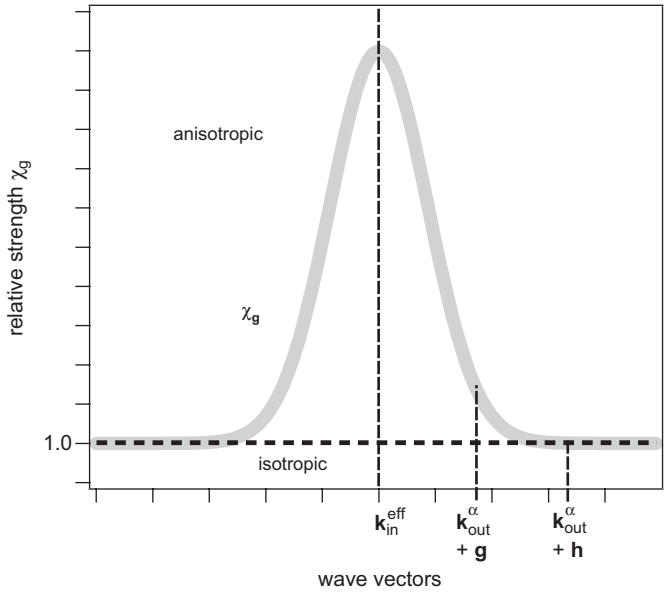

Fig. 2. Description of the different relative strength of inelastic scattering into directions $\mathbf{k}_{\mathrm{out}}^{\alpha} + \mathbf{g}$ and $\mathbf{k}_{\mathrm{out}}^{\alpha} + \mathbf{h}$ as a function of deviation from forward scattering into direction $\mathbf{k}_{\mathrm{in}}^{\mathrm{eff}}$.

In this equation, $\mathbf{q} = \mathbf{k}_{\mathrm{out}}^{\alpha} - \mathbf{k}_{\mathrm{in}}^{\mathrm{eff}}$. The phenomenological parameters a, b, and $\mathbf{k}_{\mathrm{in}}^{\mathrm{eff}}$ have to be chosen for best agreement with the experiment. The factor $\chi_{\mathbf{g}}$ describes the deviation from isotropic scattering which is obtained by setting all $\chi_{\mathbf{g}} = 1$. This is shown in Fig. 2.

Finally, a refined version of Eq. (5) results:

$$I_{\mathrm{DYN}}^{\mathrm{ED}}(\mathbf{k}_{\mathrm{in}}^{\mathrm{eff}}, \mathbf{k}_{\mathrm{out}}^{\alpha}) \propto A \sum_{n,ij} Z_n^2 B^{ij}(t) \sum_{\mathbf{g},\mathbf{h}} \chi_{\mathbf{g}} \chi_{\mathbf{h}} C_{\mathbf{g}}^{(i)} C_{\mathbf{h}}^{(j)*} \exp(-M_{\mathbf{g}-\mathbf{h}}^n) \exp[\mathrm{i}(\mathbf{g}-\mathbf{h})\cdot\mathbf{r}_n] \tag{8}$$

This simplified model shows the basic properties necessary for the appearance of excess–deficiency features in a transparent way without increasing the computational load beyond practical limits. The extension to more realistic models should be straightforward. Especially, it does not need to be assumed that the inelastic scattering is rotationally symmetric with respect to an axis defined by $\mathbf{k}_{\mathrm{in}}^{\mathrm{eff}}$. More complex models, however, require the introduction of additional parameters, the significance of which cannot be estimated at the moment without further experimental and theoretical analysis. In the most general type of approach, the elastic and inelastic redistribution of electrons from the states of the incoming beam into the states of the detected electrons needs to be considered [10–12]. Our aim here is, however, to explain and apply the basic mechanism using a phenomenological model that represents relevant physical properties of the observed processes without relying on the exact microscopic details.

Having presented the theoretical model, we will show a prototypical result of simulations applying Eqs. (7) and (8) in the next section.

4. Results and discussion

For the calculation of the GaN backscattering pattern, 610 reflections with a minimum lattice spacing $d_{hkl} = 0.35\,\text{Å}$ and a minimum structure factor amplitude of $U_{\min} = 0.008\,\text{Å}^{-2}$ have been taken into account. All other relevant parameters were the same as in the previous investigation [3]. In addition, for the excess–deficiency parameters we used $a = 10^3$, $b = 4.8\,\text{Å}^{-1}$ and

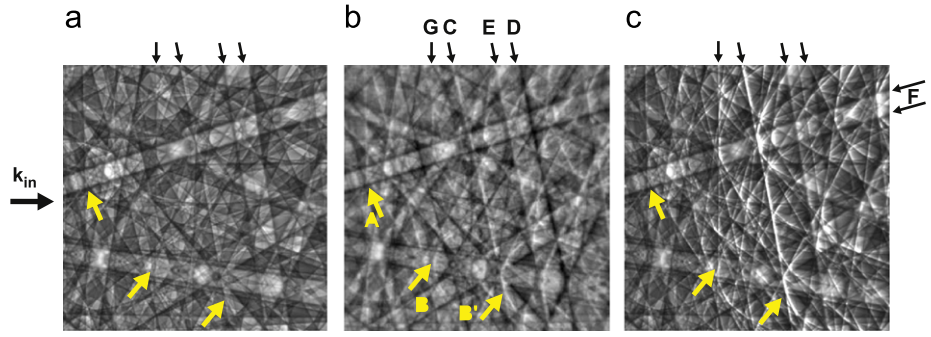

Fig. 3. Simulated patterns of GaN(0 0 0 1) at 20 kV for an isotropic inelastic source (a) and anisotropic source (c) which shows the appearance of excess- and deficiency features that are observed in the experimental pattern [3] (b). In the right panel, the excess–deficiency effects are intentionally exaggerated for better visibility of the qualitative changes.

$\mathbf{k}_{\mathrm{in}}^{\mathrm{eff}} = [-2, 12, 6]$. This direction corresponds to an incident beam from the left of Fig. 3. There we show the results of simulations with (Fig. 3c) and without (Fig. 3a) the excess–deficiency model in comparison to an experimental pattern (Fig. 3b). The choice of parameters leads to a somewhat exaggerated excess–deficiency effect which we chose for better visibility of the qualitative differences that are created with respect to the isotropic case.

We note that in the isotropic simulation (a), all the main features of the pattern are correctly reproduced. Especially, we note the appearance of higher order Laue zone (HOLZ) rings (features *A* and *B* in the experimental pattern). However, in comparison with the experiment, this simulation for instance is unable to reproduce the asymmetry between features *E* and *D* and also the bright line *C* does not show up as prominent as in the experimental pattern.

When the calculation is done with the anisotropic source model, we nicely see the illumination-like effect coming from the left. Now, line *C* shows up brightly also in the simulation, and line *D* is darker than the excess line *E*. Most interestingly, the HOLZ features *A* and *B* show up more clearly and match much better with experiment.

The simulation reproduces another characteristic property of the experimental patterns correctly, namely that not all Kikuchi lines are affected equally by the excess–deficiency effect. Lines running parallel to the incidence direction are not showing the effect (e.g. the lines along *F*). This becomes clear from the qualitative discussion in Section 2: The scattering directions of the corresponding pairs of reflections differ predominantly in their position parallel to $\mathbf{k}_{\mathrm{in}}^{\mathrm{eff}}$. There is a considerably reduced anisotropy in this case because of the assumed rotational symmetry of the inelastic scattering strength around $\mathbf{k}_{\mathrm{in}}^{\mathrm{eff}}$. This means there is a strong right–left anisotropy and a much lower top–bottom anisotropy in Fig. 3.

The model correctly reproduces the excess–deficiency effect as a property of a specific reflection corresponding to a *line* in the pattern rather than as a property of a scattering direction corresponding to a single *point* on the detection screen. What is important to realize is that the *a priori* symmetrical dynamical scattering from a pair of $\mathbf{g}$ and $-\mathbf{g}$ reflections in Fig. 1 directly translates the anisotropy in the plane of *A* and *B* into an excess–deficiency anisotropy of the Kikuchi line pair that runs perpendicular to $\mathbf{k}_{\mathrm{in}}^{\mathrm{eff}}$ on the screen.

The limits of our simplified model are seen, for example, in the fact that the line *G*, which appears prominently in the simulation, is only very weakly visible (in fact barely discernible) in the experiment. For a quantitative description of EBSD, one would probably need a more refined model than Eqs. (6) and (7) provide. For this, it would be necessary to experimentally analyze the effective angular anisotropy of the inelastic scattering more closely. Systematic variation of the incidence angle in an EBSD experiment and the measurement of the resulting excess–deficiency features could provide more insight into the functional dependence of the effective anisotropy. In this way, it might be possible to quantify for example the influence of the excess–deficiency features on lattice parameter determinations. Another type of approach would be to identify experimental situations in which the excess–deficiency asymmetries are suppressed considerably. From our model, this should be the case for detection directions towards 180° backscattering, where at the same time, however, also smaller signals are observed.

As mentioned in the Introduction, another highly important aspect of inelastic scattering in EBSD concerns the energy spread of the backscattered electrons. The corresponding spread of electron wavelengths directly limits the resolution and contrast of the experimental diffraction patterns [13]. For a quantitative analysis of EBSD patterns, it is important to analyze how this limits the possible information. It is straightforward to integrate the effect of the electron energy spectrum on the level of our current simulations. By using Monte–Carlo simulations for the calculation of the inelastic electron spectrum and adding the corresponding dynamical electron diffraction patterns according to this spectrum, one could obtain important estimations of the influence of the energy broadening. Preliminary calculations indicate that this clearly results in a loss of fine structure from high order Kikuchi lines which sensitively change their position with energy and thus tend to average out if an extended range of wavelengths is present. An extended analysis using realistic energy spectra will be the topic of a future paper.

5. Summary

We presented a model that describes the appearance of excess and deficiency features in EBSD patterns and their inclusion in many-beam dynamical simulations. The excess and deficiency features appear naturally if we take into account the anisotropy of the internal sources of inelastically scattered electrons which are subsequently scattered elastically to produce the EBSD pattern. Inclusion of this effect in our dynamical simulations results in an improved agreement with experimental measurements.

Acknowledgements

I would like to thank C. Trager-Cowan, A.P. Day, A. Wilkinson, and D. Dingley for inspiring discussions during the UK EBSD meeting in 2007 at New Lanark, Scotland.

References

[1] A.J. Schwartz, M. Kumar, B.L. Adams (Eds.), Electron Backscatter Diffraction in Materials Science, Kluwer Academic Publishers/Plenum Press, New York, 2000.
[2] A.J. Wilkinson, P.B. Hirsch, Micron 28 (1997) 279.
[3] A. Winkelmann, C. Trager-Cowan, F. Sweeney, A.P. Day, P. Parbrook, Ultramicroscopy 107 (2007) 414.
[4] J.B. Pendry, Low Energy Electron Diffraction: The Theory and Its Application to Determination of Surface Structure, Academic Press, New York, 1974.
[5] J.C.H. Spence, J.M. Zuo, Electron Microdiffraction, Plenum Press, New York, London, 1992.
[6] C.J. Humphreys, Rep. Prog. Phys. 42 (11) (1979) 1825.
[7] Y. Kainuma, Acta Cryst. 8 (1955) 247.
[8] C.J. Rossouw, P.R. Miller, T.W. Josefsson, L.J. Allen, Philos. Mag. A 70 (6) (1994) 985.
[9] C.R. Hall, P.B. Hirsch, Proc. R. Soc. London A 286 (1965) 158.
[10] C.J. Rossouw, Ultramicroscopy 16 (1985) 241.
[11] S.L. Dudarev, L.M. Peng, M.J. Whelan, Phys. Rev. B 48 (1993) 13408.
[12] S.L. Dudarev, P. Rez, M.J. Whelan, Phys. Rev. B 51 (1995) 3397.
[13] A. Deal, T. Hooghan, A. Eades, Ultramicroscopy 108 (2008) 116.